Chapter 4. Reactive Extrusion in a High Throughput Parallel Co-rotating Twin-Screw Extruder- Scale-up Considerations and Foam Generation by Supercritical CO_2

4.1 Abstract

Twin-screw extruders offer a viable process tool for conducting reactive processes like polymerization or polymer-polymer compatibilization in a continuous mode. In this study a unique reactive chemistry for compatibilizing starch and PCL polymers was scaled up from a batch-type, low output (0.2 kg/hr) conical twin-screw co-rotating micro-extruder (length/diameter, L/D =5) to a continuous high output (~3-6 kg/hr) parallel twin-screw co-rotating extruder (Wenger TX-52). Screw speed, configuration and feed rates were optimized to achieve desired PCL-like elongation of reactive blends. Similar specific mechanical energies (SME's) were obtained when the TX-52 was operated at screw speeds $1/3^{rd}$ of that in the micro-extruder. Higher screw speeds resulted in polymer shear degradation and lower mechanical properties. Smooth extrudates without steam expansion were obtained in the TX-52 at low feed rates. At high feed rates/outputs, mechanical properties of extrudates were lower than those at low feed rates/outputs. A series of forward kneading discs staggered at 30^0 angles and located in the first heating zone was found to result in mechanical properties comparable to those from micro-extrusion.

4.2 Introduction

In the industry, reactive processing of biodegradable polymers is generally done by continuous twin-screw extrusion (1-5). Compared to single screw extruders, twin-screw extruders provide higher throughputs, better temperature control, adjustable residence time distribution and continuous stable flow through the die (6). The

availability of a continuous twin-screw extruder in the Food Process & Development Lab (FPDL) provided an opportunity for studying the scaling process. This chapter will describe the scaling up process and optimization in a continuous commercial level twin-screw extruder. A Wenger TX-52 from Wenger Inc, USA was the extruder in which the scale-up was done. The challenges in scaling up from a small bench-top extruder to a high throughput extruder like TX-52 are illustrated in Table 4.1. The length-to-diameter (L/D) ratio was atleast 3 times higher while the operating output was atleast 15 times higher in TX-52 compared to the micro-extruder. Photographs of the two extruders are given in Figure 4.1. An important criterion for evaluating the success of scale-up process was the mechanical properties of extrudates. The characteristic PCL-like tensile elongation of micro-extruded samples must also be exhibited by TX-52 extrudates. The target mechanical properties obtained in a micro-extruder are given in Table 4.2. The reactive formulation (STPCLPER-6) has similar elongation as 100% PCL while the non-reactive formulation (STPCL) (formulation in chapter 3, Table 3.1) breaks off at early strains.

To accomplish a successful scale-up, it was essential to understand the mechanism of polymer melt flow and obtain the same set of reactions and flow in both the extruders. Fundamental extrusion studies have identified several independent process variables that affect melt flow and final material properties. Some of these variables may affect the reactive extrusion process in our studies while others may not. Thus a rationale for variable selection has been developed and discussed in the following paragraphs. It was expected the optimum values of parameters in both the extruders would be different.

Table 4.1: Specifications of conical twin-screw micro-extruder and parallel twin-screw Wenger TX-52

Extruder Parameters	**Micro-extruder**	**Wenger TX-52**
Length/Diameter (L/D)	5*	27 or 15
Diameter of Screw (mm)	19*	52
Operating Throughput (kg/hr)	0.2	3-30
Maximum Motor Horsepower (HP)	0.3	50
Operating Temperature (^{0}C)	120	122$\pm$5
Maximum Rated Screw Speed (RPM)	360	355

*Numbers denote average diameter values of screws from top to bottom in the vertical conical micro-extruder

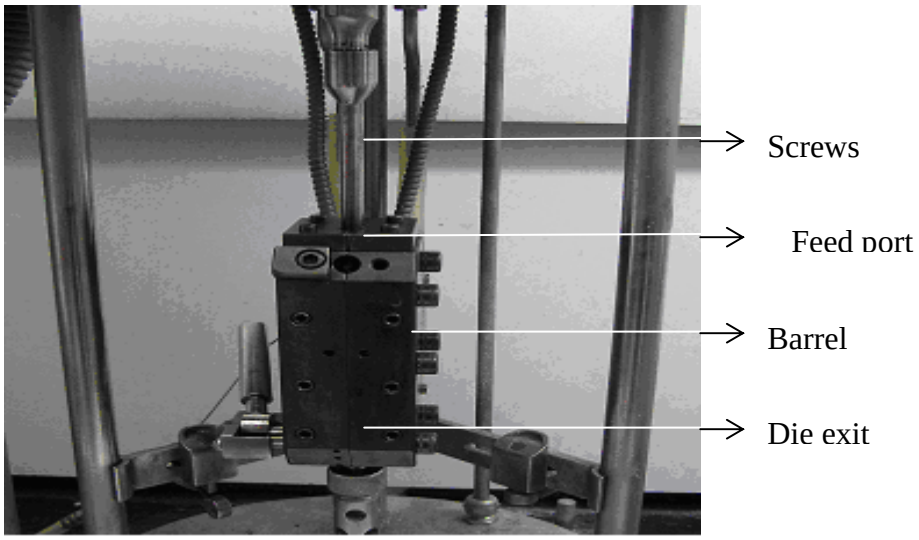

(a)

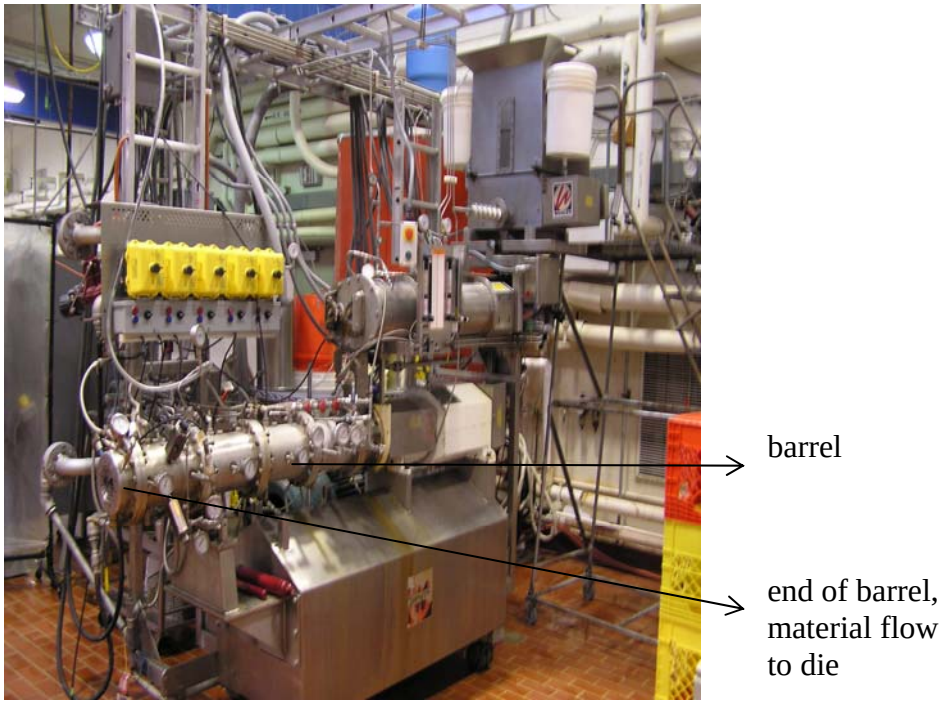

(b)

Figure 4.1: Photographs of twin-screw co-rotating (a) conical, vertical micro-extruder and (b) horizontal and parallel Wenger TX-52 extruder

Table 4.2: Tensile properties of starch-PCL blends from micro-extrusion and injection-molded into standard dog-bone shapes

Material	**Max. Tensile Strength, MPa**	**Ultimate Elongation, %**	**Tensile Modulus at 1% Strain, MPa**
100% PCL	30.8	1163	303.3
STPCL (non-reactive extrusion)*	12.6	265	211
STPCLPER-6 (reactive extrusion)*	15.8	1010.5	206.8

* Formulations in chapter 3, Table 3.1

4.2.1 Bench-Top Micro-extrusion

Reactive extrusion processes discussed in previous chapters were done on a vertical co-rotating conical twin-screw micro-extruder (DACA Instruments, Goleta, CA-USA). A photograph of the micro-extruder is given in Figure 4.1-a. Premixed ingredients in the form of free-flowing powder were fed to the micro-extruder with the die exit closed. The die was circular in shape with diameter and length of 2.8 mm and 16 mm respectively. The barrel temperature and screw speed were set at 120^0 C and 120 rpm respectively. The typical filling weight of the micro-extruder was about 7-8 grams of formulation. Once the extruder was filled, residence time was varied between 1-3 minutes before the die was opened. Thus the extruder was completely filled during the micro-extrusion studies. As seen in Figure 4.2, when the die was kept closed there was constant recirculation of material inside the barrel. The material or polymer melt

traveled downward with the rotation of screws and once it reached the bottom, it re-circulated back to the top when the die was closed. When the die was opened, the material flowed out of the die, with no more recirculation. The extrudates were cylindrical shaped and were then injection-molded for further tensile characterizations. Our micro-extrusion studies were batch processes whereas TX-52 and commercial extrusions in the industry were continuous processes.

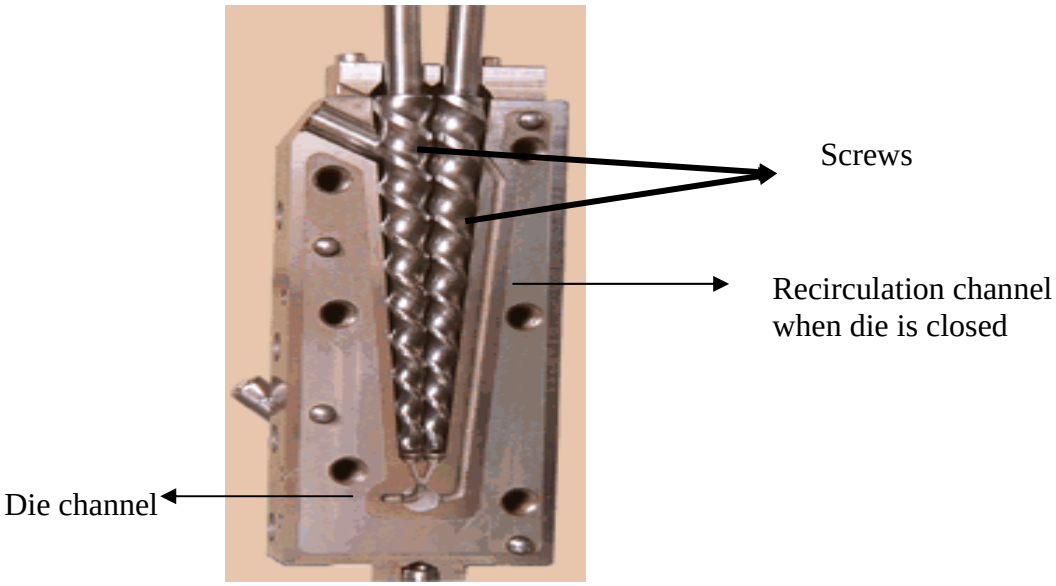

Figure 4.2: Recirculation and die flow channels for polymer melts in the twin-screw conical micro-extruder. Material flow from top to bottom

4.2.1.1 Screw Configuration in the Twin-Screw Micro-Extruder

The barrel and screw configuration in the micro-extruder are shown in Figure 4.3. Considering an average diameter of screws from tip-to-tip, the average L/D (screw length-to-diameter) ratios of for the micro-extruder was calculated as 5:1. Correspondingly both the screws were decreasing in diameter as it moved from feed side towards the die (from top to bottom in figure 4.2). Figure 4.3 also shows the

intermeshing nature of screws. Intermeshing screws help to circulate material from one screw to another leading to better mixing.

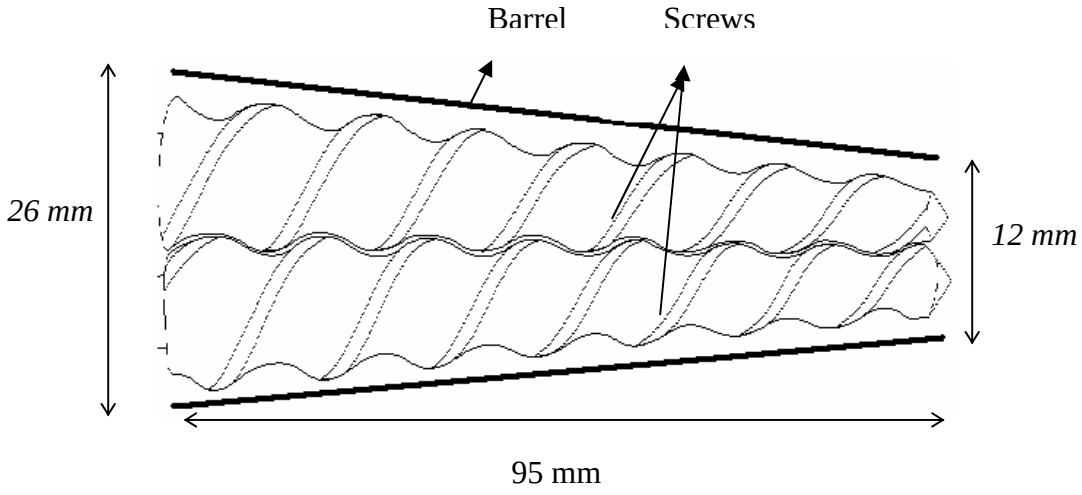

Figure 4.3: Dimensions of the conical twin-screw micro-extruder. Screws shown in horizontal plane.

Tadmor *et al* (7) have discussed the effect of screw geometry and screw speed on melt flow behavior. Zuilichem e*t al* (8) have reviewed the many types of screw geometries available that are typically used in the extrusion industry. Screw geometries and speed will affect pressure profile in the extruder, shear rates, residence time distribution (RTD), melt viscosities, melt temperature and polymer molecular integrity during extrusion. Many studies have been done on polymerization processes in twin-screw extruders (2,3,5,9-12). The type of screws used and screw speed were found to affect reaction kinetics, % monomer conversion, occurrence of undesirable side reactions, melt temperature and mean residence time. Thus choosing a right screw design was

important for a successful scale-up. From the following paragraphs, it will be clear that optimum screw designs in two extruders of different scales need not be identical.

4.2.2 High Output Continuous Extrusion

Wenger TX-52 is a continuous parallel horizontal co-rotating and intermeshing twin-screw extruder. The number 52 stands for the diameter of the screw. Figure 4.4 shows a schematic of TX-52 extruder set-up. Formulations in the form of powder are filled in a single screw feed system known as the feed hopper or live bin. From the feed hopper the powder was conveyed through a twin-screw pre-conditioner. From the pre-conditioner the material flowed into the extruder barrel. The extruder barrel contained the two screws that were rotated by a 50 HP motor configured with a gear-box. Figure 4.4 also shows the classification of entire extruder barrel length into four different heating zones or heads. The heating zones started from the end of feed screw section (156 mm long) and the length of each head or heating zone was 312 mm. The TX-52 is an ideal system for the scale-up process since it closely resembles typical commercial twin-screw extruders. It is also a versatile system in which the degree of mixing could be varied by using suitable segmented screw configurations. Also the number of heads could be decreased from 4 to 2 thus reducing the L/D ratio from 27 to 15. The speed of the single screw feeder could also be varied to obtain variable feed rates. The extruder was equipped with a jacketed heating/cooling system in which high-pressure steam or cold fluid can be circulated to obtain high/low temperatures.

4.3 Experimental

There are several independent process variables in an extrusion process that affects flow behavior and material properties. Their effects on material properties and

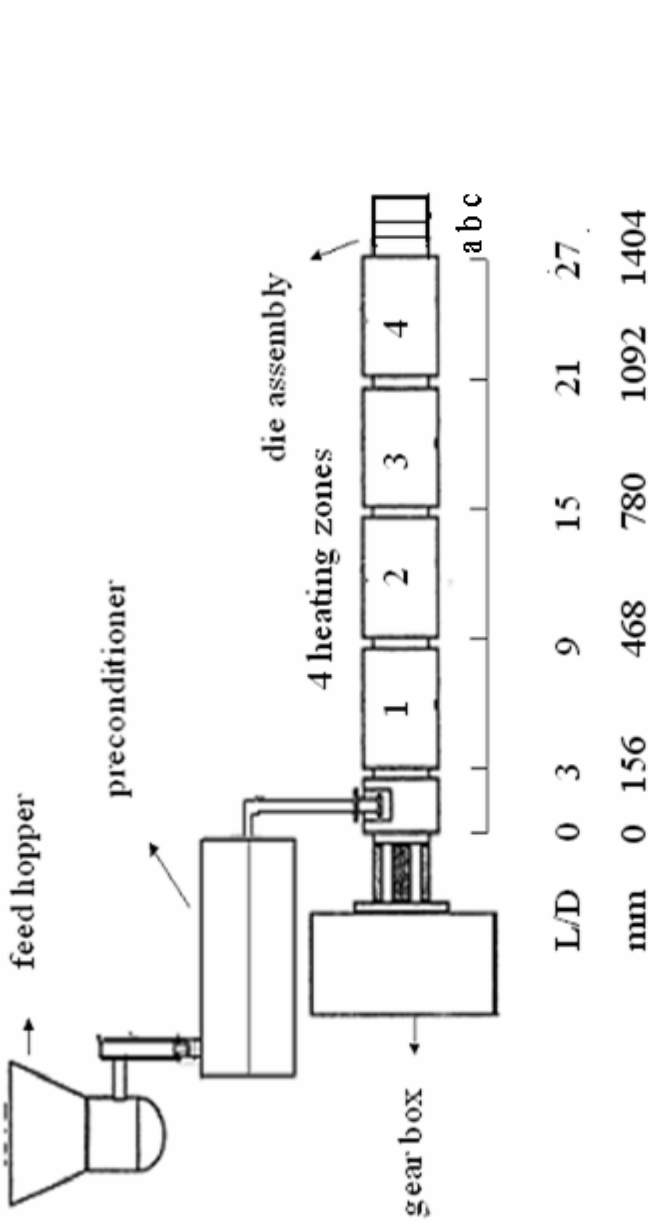

Figure 4.4 : Set-up of Wenger TX-52 Extruder. Die assembly consisted of a) head plate of length, (L)=23 mm followed by b) spacer and c) die holder of lengths 12 mm and 25 mm respectively

polymer flow behavior in general during extrusion were reviewed by many authors (2,3,9-12). The variables are temperature, feed rate or extruder output, extruder L/D ratio, die dimensions, screw speed, screw configuration or types of mixing elements used and composition of formulation. In our extrusion process, the temperature was always kept at 122 $\pm$ 5 ^{0}C in all the heating zones and a single formulation (STPCLPER-6) was used. Dies with sufficiently large cross-sectional area were selected so that low shear rates (< 100 s^{-1}) were obtained in the die (see Table 4.7). Two levels (minimum and maximum) for the remaining variables were chosen in order to minimize the number of experiments. The experimental design was based on a model developed by Mange *et al* (13). The selected variables were:

a) Extruder Output (Parameter X1): Low level (-) = 3-6 kg/hr, High level (+) = 20-35 kg/hr. The minimum set-point feed rate in the TX-52 was 15 kg/hr. In order to achieve lower feed rates and thus lower outputs, part of material coming from pre-conditioner was diverted out and re-circulated. Actual ouputs from the extruder were evaluated by weight measurements. It was observed that lower feed rates were less stable than higher rates. Surging flow from the die because of variable flow rates was observed at times especially when the extruder was operated for long periods of time at low feed rates. An average of 2-4 replicates was taken to measure actual extruder outputs.

b) Screw speed (Parameter X2): Two levels of screw speed were used. Low level (-) = 40 rpm and high level (+) = 90 rpm. The actual screw speeds were approximately 5 rpm higher than the set-points.

c) Screw configuration (Parameter X3): Two types of screw configurations were used. One consisted entirely of forward screw elements (F) and the other (M) consisted of both forward screw elements and 6 kneading discs or paddles. Figure 4.5 (a-d)

illustrates ‘F’ and ‘M’ configurations for L/D ratios of 15:1 and 27:1. All the configurations started with two feed screws on each shaft as shown in Figure 4.5-a. The heating zones started from the end of feed screw section and the length of each head or heating zone was 312 mm (see Figure 4.4). As seen in Figure 4.5-a and b, the ‘F’ configuration consisted of forward screw elements. Two screws of different pitches were used in ‘F’ configuration. One had a pitch of 26 mm and another had a pitch of 19 mm. The ‘M’ configuration (Figure 4.5-c and d) consisted of the above two forward screws and also a 6-unit kneading disc or paddles. The paddles are arranged at a forward staggering angle of 30^0 relative to each other. This is illustrated in Figure 4.5-e. For the L/D ratio of 15, these discs were located near the feed side whereas the discs were located more downstream for the L/D ratio of 27.

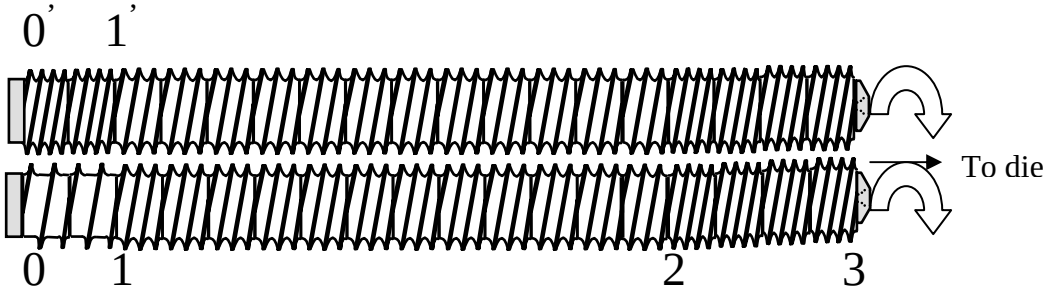

0-1: Feed screws of pitch (P)= 38 mm and length (L)=156 mm, 0'-1': feed screw of P= 19 mm and L=156, 1-2: screws of pitch (P) 26 mm and length (L)= 936 mm, 2-3: screws of P= 19 mm and L=312 mm

(a)

Figure 4.5: Forward screw configuration (F) for (a) L/D= 27, (b) L/D=15 and Mixed screw configuration (M) for (c) L/D= 27 and (d) L/D = 15. 4.5-e shows forward kneading discs that are staggered at an angle of 30^0. The Figures are shown as non-intermeshing eventhough the actual screws are intermeshing. Numbers below the screws in Figures 4.5-a to c indicate the end of screws of a particular type and the beginning of another.

Figure 4.5 (continued)

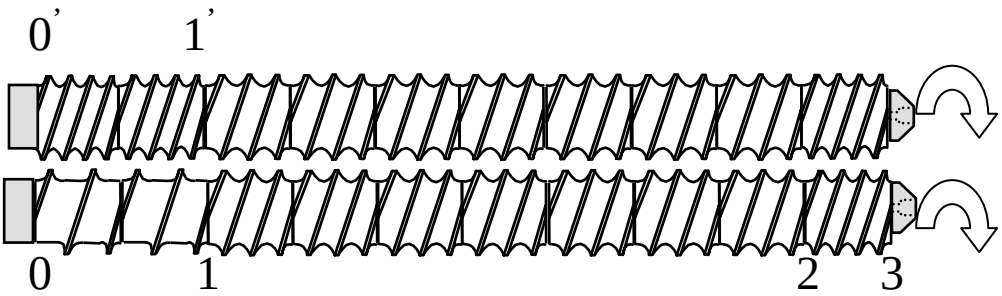

0-1: feed screw of L=156 mm, 0'-1': feed screw of P= 19 mm and L=156, 1-2: screws of P=26mm and L=546 mm, 2-3: screws of P=19mm and L= 78mm

(b)

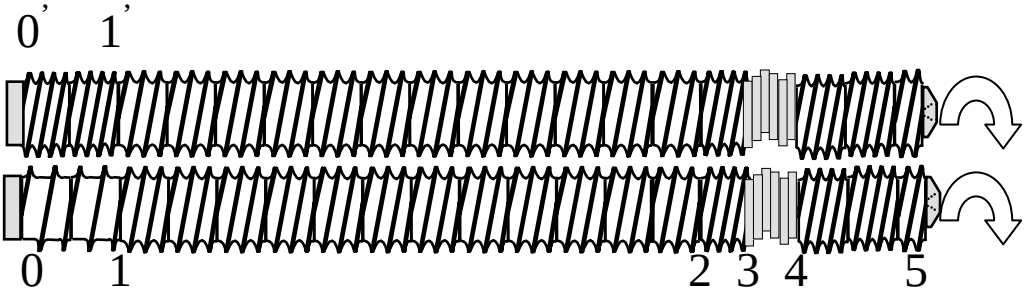

0-1: feed screw of L=156 mm, 0'-1': feed screw of P= 19 mm and L=156, 1-2: screws of P=26mm and L=936 mm, 2-3: screws of P=19mm and L= 78mm, 3-4: kneading discs of length 36 mm, 4-5: screws of P=19mm and L=198mm

(c)

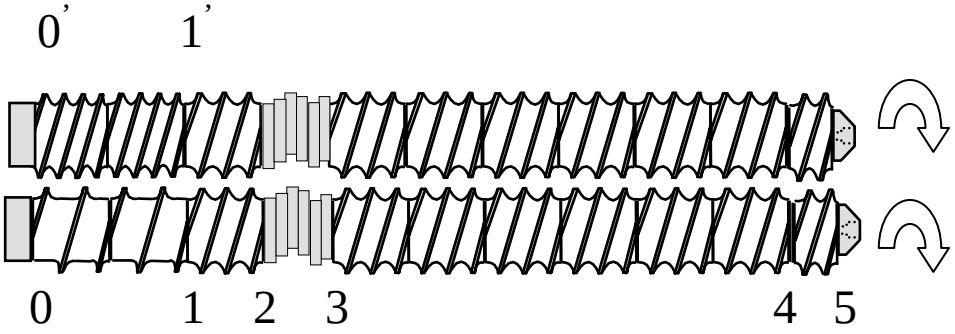

0-1: feed screw of L=156 mm, 0'-1': feed screw of P= 19 mm and L=156, 1-2: screws of P=26mm and L=78 mm, 2-3: kneading discs of L=36mm, 3-4: screws of P=26mm and L= 468mm, 4-5: screws of P=19mm and L=42mm

(d)

Figure 4.5 (continued)

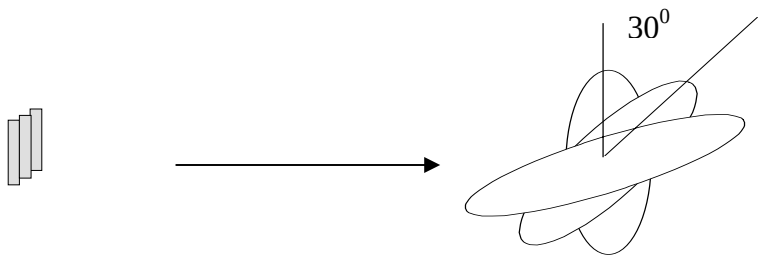

(e)

d) L/D ratio (Parameter X4): Low level (-) L/D =15 and high level (+) L/D =27. L/D of 15 was achieved by removing the last two heads (head #'s 3 and 4 in Figure 4.4). Thus there were 4 heating zones for L/D =27 and 2 for L/D=15. Table 4.3 illustrates the various experiments carried out at different levels of above process variables.

Table 4.3: Experimental plan for the scale-up of reactive extrusion process to TX-52

Experiment #	**Feed Rate, X1**	**Screw Speed, X2**	**Screw Configuration, X3**	**L/D ratio, X4**
1	+	-	F	+
2	-	-	F	+
3	-	+	F	-
4	-	-	F	-
5	-	-	M	-
6[a]	+	-	M	+

a- Circular dies of 12 mm diameter used, rest- 2x38 mm^2 slit dies, feed rate (+)= 20-35 kg/hr, (-) = 3-6 kg/hr, screw speed (+)=90rpm, (-)=40rpm, screw configuration (F)= forward screws, (M)= forward screws and kneading discs, L/D ratio (+) = 27, (-)=15.

4.3.1 Materials

Native wheat starch (MIDSOL 50, Midwest Grain Products, Atchison-KS, USA) had the following solids composition-98.5% carbohydrates, 1% lipids, 0.2% proteins and 0.22-0.25% ash. TONE P787 (Dow Polymers, Danbury, CT, USA) is a 80,000 molecular weight ($M_{n,average}$) polycaprolactone (PCL) polymer of melting point 54^0C and available as pellets. These pellets were cryogenically ground into powder in which 98% of particles were <600μm. Glycerol (Kosher Superol, Procter & Gamble Chemicals, New Milford, CT, USA) was atleast 99% pure. Nanocor I.30E organoclay (Nanocor Inc., Arlington Heights, IL) is of montmorillonite (MMT) type with sodium ions (Na^+) replaced by quaternary ammonium octadecyl cations ($C_{18}H_{35}$ NH_4^+). Hydrogen peroxide (>90wt% purity, FMC corporation, Pasadena, TX-USA) and ferrous sulfate catalyst (Fischer Scientific, Fairlawn-NJ, USA) were constituents of Fentons reagent. The formulation used was STPCLPER-6 (starch:PCL:glycerol:clay weight ratio= 1:1:0.5:0.16; H_2O_2(30% solution basis)= 0.067 ml/g of starch; Fe^{2+} catalyst=0.0025 g/g starch).

4.3.2 Methods

4.3.2.1 TX-52 Extrusion

Appropriate amounts of powder ingredients (starch, PCL and clay) were mixed in a tumble mixer. Glycerol and hydrogen peroxide were subsequently mixed with the dry powder mix in a high-speed knife mixer. The resulting mixture was screened manually to obtain a uniform size material without any large lumps. This material was then left overnight and subsequently mixed with ferrous sulfate catalyst before beginning extrusion experiments. All process variables in the extruder were controlled using an electronic interface. Constant feed rates were maintained on volumetric basis i.e. the

system required bulk density as input parameter for ensuring set point feed rates. Also the pre-conditioner only served as an extra conduit before the powder entered the extruder barrel.

Temperatures in all the heating zones were maintained at 122 $\pm$ 5^0C using high-pressure steam (30-40 psi) flowing through the jackets around the extruder barrel. The cross-sectional dimensions of slit and circular dies were 2 x 38 mm^2 and 12 mm (diameter) respectively with die land length of both the dies being 10 mm. Die dimensions are illustrated in Figure 4.6. The die assembly (shown in Figure 4.4) consisted of a head plate followed by the spacer and die holder. The head plate had a circular flow cross-section with two flow channels on the upstream side receiving the melt from the end of two screws that converged to a single cylindrical flow channel downstream supplying melt to the spacer and dies. A red dye (Red #40) was used to measure residence times of melts in TX-52. Minimum residence time (R_{min}) was calculated as the time interval between addition of dye where feed from pre-conditioner entered the extruder barrel and its appearance in the product from the die.

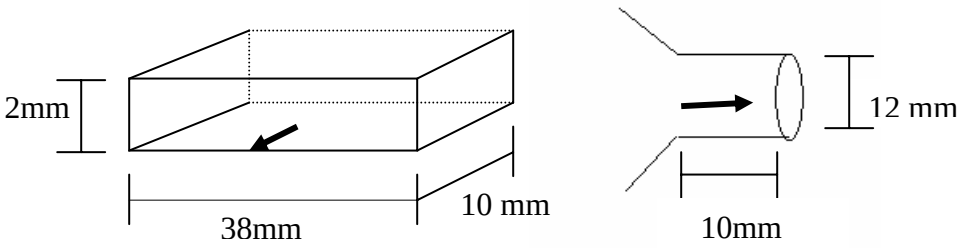

Figure 4.6: Die shapes and dimensions used in TX-52, a) slit die, and b) cylindrical die. Black arrows indicate direction of material flow

Product temperature at die exit was measured using a hand-held thermocouple before and after samples were collected. All measurements and sample collections were done approximately 15-20 minutes after first appearance of product from the die to ensure stable operation of the extruder.

Specific mechanical energy (SME) was a measure of mechanical energy applied to the polymer melt by the rotation of screws. SME during extrusion in the TX-52 was calculated as follows (14):

$$\text{SME (kJ/kg)} = \frac{Load_{motor} P_{motor} \omega}{\omega_{max} \dot{m}} \qquad \text{(i)}$$

P_{motor} is power of motor driving the screws= 50 HP (37.3 kJ/s),

ω is screw speed, revolutions per minute

ω_{max} is maximum rated screw speed in TX-52, 355 revolutions per minute

$\dot{m}$ is mass flow rate in kg/s

$Load_{motor}$ is % load on motor.

Scanning electron microscopy (SEM) was used to analyze the cellular structure of foams produced by injection of supercritical CO_2 (SC-CO_2) during extrusion. The samples were analyzed with a Leica 440 scanning electron microscope (Leica Microsystems Inc, Bannockburn, IL) at electric field strength of 25 kV and 41x magnification. PCL crystallinity and melting point in extruded samples were analyzed by differential scanning calorimeter (DSC) using methods described in chapter 2 (section 2.4.5). Clay dispersion behavior in extruded samples was studied by wide-

angle x-ray diffraction using parameters described in chapter 2 (section 2.4.4). Extrudates from TX-52 were injection molded in a micro-injector whose barrel temperature was kept at 140^0 C-150^0C and mold temperature at ambient. Tensile measurements of dog-bone pieces were done on an Instron 1122 (Instron Corp., Canton-MA) universal tester at a crosshead speed of 50mm/min. Maximum stress and % elongation at rupture were measured.

4.4 Results and Discussion

Table 4.4. illustrates the effect of feed rate, screw speed, screw configuration and L/D ratio on tensile properties, SME, residence time and product temperature. As a comparison material properties and process parameters from micro-extruder are also listed.

4.4.1 Effect of Feed Rate and Extruder Output (Parameter X1)

High feed rates and high outputs consistently gave poor products in terms of appearance and tensile properties. Steam expansion was seen in extrudates coming from the die at high feed rates, at both L/D ratios of 15 and 27. Figure 4.7 illustrates products obtained at low and high feed rates with steam bubbles seen in samples at higher feed rates (Figure 4.7-a). Table 4.4 illustrates tensile elongation and strength, SME and product temperature at both high (experiment#1) and low feed rates (experiment#2). The tensile properties were poor compared to products obtained from micro-extruder. Tensile properties of extrudates obtained at lower feed rates were significantly higher than those obtained at higher feed rates.

Table 4.4: Effect of different experimental variables in TX-52 on dependent process variables and extrudate tensile properties. A comparison of micro-extrusion properties is also listed in the bottom.

Experiment #	**Ultimate Elongation, %**	**Maximum Tensile Strength, MPa**	**SME, kJ/kg**	**Minimum Residence Time R_{min} , s**	**Product Temperature, ^{0}C**
1	278[a]	4.1[a]	nm	94	136
2	524[b]	6.0[b]	218.8[a]	80	142
3	114[c]	4.2[a]	599.6[b]	270	141
4	732[d]	7.9[c]	233.6[c]	123	128
5	1028[e]	12.9[d]	291.8[d]	120	129
6	1061[e]	12.2[d]	422.4[e]	nm	110
Micro-extruder	~1100[e]	13-14[d]	232.0[a,c]	74	120

nm- Not measured, same alphabet means no significant difference at α=0.05

4.4.2 Effect of Screw Speed

Screw speed affected the mechanical properties of extrudates significantly. Table 4.4 shows the effect of screw speed (experiment#'s 3 and 4) on dependent process parameters (SME and product temperature) and mechanical properties. Screw speed was expected to affect SME and product temperature by generating higher viscous dissipation at higher speeds. The relation between speed and SME was given in

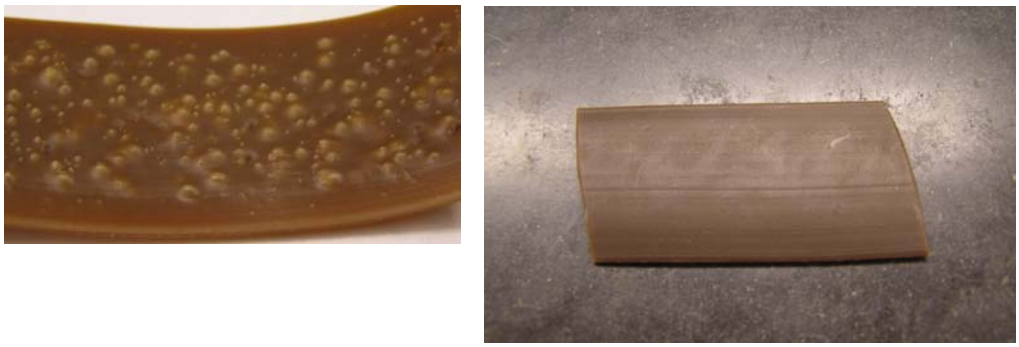

(a) (b)

Figure 4.7: Effect of feed rates on extrudate appearance, (a) steam bubbles seen at high feed rates (experiment #1) and (b) smooth extrudates at low feed rates (experiment#2)

equation (i). Viscous dissipation is given by the following equation (15):

Viscous Dissipation (W/m^3), $q_v = K \dot{\gamma}^{1+n}$ (ii)

K ($Pa\text{-}s^n$) and n are consistency coefficient and power law index from the power law model and $\dot{\gamma}$ is shear rate (s^{-1}). Thus for a given polymer melt higher screw speeds resulted in higher shear rate and subsequently higher viscous dissipation. Thus the extrudate product temperature was higher in experiment # 3 (higher screw speed) than in # 4 (lower screw speed).

The minimum residence time was higher at higher screw speeds because the feed rate in experiment # 4 was 3.0 kg/hr while that of #3 was 2.3 kg/hr. As mentioned before high screw speeds led to high SME's according to equation (i). SME for experiment # 3 was significantly higher than that in # 4. Other studies have observed higher polymer degradation, especially starch, under high SME's. For example, Martin *et al* (16) reported that starch depolymerization was initiated at >360 kJ/kg. We expect this threshold to be lower in our studies because of harsh reactive extrusion conditions in

the presence of hydrogen peroxide. Thus larger degree of starch degradation at higher screw speeds contributed to lower properties.

4.4.3 Effect of Screw Configuration

For STPCLPER-6 formulations and forward screw configurations (F), the mechanical properties were significantly lower than the micro-extruded products independent of the feed rate. This is shown in Table 4.4 for experiment # 1,2,3 and 4. In chapter 2 it was reported that nanoclay was essential to obtain improved properties at the extrusion temperature of 120^0C. Absence of nanoclay at this temperature led to poor material properties. It was postulated that nanoclay played a critical role during the initial reaction stages when the polymers and peroxide were exposed to warm temperatures. Thus a greater degree of mixing was required among all the ingredients-PCL, starch, clay, glycerol, peroxide and catalyst- in the initial stages when the formulation was exposed to warm temperatures in the first head of TX-52. This postulate was tested by using forward screw configuration (F) with higher amounts of nanoclay (9wt% and 12wt%). Thus higher amounts of nanoclay would compensate for the low degree of mixing with F configuration. Table 4.5 shows the difference in properties at 6, 9 and 12wt% nanoclay for experiment#4. Elongation and strength in 9 and 12% clay formulations were significantly higher than 6% clay. Eventhough the 9 and 12% formulations were not equivalent to material properties from micro-extrusion, better properties at higher nanoclay levels indicated that there needed to be better mixing during the initial heating period.

In order to improve the degree of mixing in the initial stages, a new screw configuration was used. This configuration (M) shown in Figure 4.5-d contained

kneading discs placed in the first heating zone to provide greater mixing than simple forward screws. The use of kneading discs have traditionally been used in plastic and food industries to provide better mixing in the extruder especially in the case of reactive extrusions (17-19). Thus the effect of mixing effectiveness or efficiency on tensile properties could be evaluated by using screw configurations F and M.

Table 4.5: Effect of nanoclay level on tensile properties and dependent process parameters for samples from experiment#4.

Nanoclay Level, wt%	**Ultimate Elongation, %**	**Maximum Tensile Strength, MPa**	**SME, kJ/kg**	**Minimum Residence Time R_{min} , s**	**Product Temperature, ^{0}C**
6%	732.4[a]	7.9[a]	233.6[a]	123	128
9%	859.9[b]	9.1[b]	283.7[a]	105	131
12%	883.5[b]	10.1[b]	340.4[b]	140	141

Same alphabet means no difference at α=0.05

Table 4.4 shows effects of F and M screw configurations on the tensile properties and process parameters of extrudates (experiment #'s 4 and 5). The best tensile properties were seen in experiment # 5, which achieved similar properties as from micro-extruder.

4.4.4 Effect of L/D Ratio

Table 4.4 illustrates the effect of low and high L/D ratios on tensile properties and dependent process parameters at low feed rates. Experiments #5 and #6 were at low

and high levels of feed rates respectively. Thus with 'M' configuration and low screw speeds, L/D ratio did not affect the mechanical properties eventhough SME's and feed rates were higher at higher L/D in experiment#6. No bubbling in extrudates was observed at higher feed rates (experiment#6) because the feed material for this test was the extrudates (cut in form of pellets) from #5. Extrudates from experiment #5 were cut into small pellets that were then fed manually for experiment #6. Unchanged tensile properties between experiment # 5 and 6 also indicated that there was no polymer degradation when the same material was subjected to two extrusion processes.

Thus overall there were three factors that were optimized for a successful scale-up:

a) Feed Rate: Lower feed rates were essential to account for moisture present in formulations. This moisture was from native starch and it was 3.7wt% for STPCLPER-6 formulations. At higher feed rates, this moisture was present in the vapor phase because of high temperature and negligible flow pressure in the extruder (120^0C and < 4 atm). The ability of vapor to escape from the feed port would depend on the filling ratio (FR) in the extruder. The fill ratio is a measure of volume of the extruder barrel that is filled with polymer melt. FR is also defined as the ratio of actual flow rate and drag flow rate by screw rotation.

$$\text{Fill Ratio (FR)} = \frac{\text{Actual Flow Rate}}{\text{Drag FLow Rate}} \qquad \text{(iii-a)}$$

An approximation for drag flow rate in twin-screw extruders is given by the equation (1, 7):

$$\text{Drag flow rate } (Q_d, \text{ m}^3/\text{hour}) = \frac{\pi \text{NDcos}\theta \text{ WH}}{2} \qquad \text{(iii-b)}$$

N is screw speed (revolutions per hour), D is diameter of screw (m) (52 mm), θ is flight angle, W is width of screw (m) and H is flight depth (m). For forward screws of pitch (L) 26 mm, W of 22.3 mm, H of 10 mm, N of 40 rpm, θ of 17.7^0 and melt density of 1204.2 kg/m^3 for STPCLPER-6 melts (from chapter 3), the total fill weight for TX-52 was approximately 50.1 kg/hr i.e. at this feed rate the extruder section containing these screws would be completely filled at 40 rpm. The values of FR's at low (-) and high (+) levels of feed rate are listed in Table 4.6. It could be seen that the degree of fill at higher levels of feed rates was atleast 6-7 times higher that at low feed rate levels. Eventhough the extruder barrel was not completely filled in both situations, at higher feed rates water vapor was not able to escape from the feed side and was carried to the die and flashed out of the extrudate (Figure 4.7-a). At lower filling ratios and feed rates there was venting from the feed port and a smooth extrudate was obtained (Figure 4.7-b).

Table 4.6: Extruder filling ratios (FR) at screw speed of 40 rpm and low/high levels of feed rate in the TX-52.

Feed Rate	**Filling Ratio (FR)**
Low Level (3-6 kg/hr)	0.06-0.12
High Level (20-35 kg/hr)	0.40-0.70

b) Screw Speed: As mentioned before screw speed affected total SME delivered by the rotation of screws to the melt. An optimum set-point screw speed of 40 rpm was found to give the best results and higher rpms led to poor tensile properties.

c) Screw Configuration: Screw configuration near the first heating zone played an important role. Kneading discs with a forward staggering angle of 30^0 and located in

the first head was expected to facilitate greater mixing among starch, PCL, peroxide and nanoclay. There are three kinds of mixing that happens in an extruder- i) axial or backward mixing, ii) radial or distributive mixing and iii) dispersive mixing. Axial mixing or back mixing occurred because of circulatory flow in the screw channel as well as pressure and leakage flows (7). Distributive mixing involves a homogenization of a mixture of two or more components and has been found to play an important role in reactive extrusion processes (19). Dispersive mixing is the break-up of cohesive agglomerates into smaller and finer particles. Kneading discs in configuration M were expected to provide greater mixing because these elements have less forward conveying ability than typical forward screws and their presence increased the degree of fill or FR. Because of these two reasons, high shear stress regions are generated within these elements thus providing greater mixing.

Since STPCLPER-6 formulation consisted of various ingredients that participate in chemical reactions, good distributive mixing was required between all the ingredients. Also material coming to the kneading discs in M was expected to be a mixture of melt and solids since the discs were located at the beginning of first heating zone. Nanoclay was initially present in the feed material in powder form of size 13 μm. These discrete particles consisted of thousands of individual platelets or clay sheets. Glass transition studies in chapter 2 indicated that nanoclay sheets acted as an effective physical barrier to cross-linking because of its high surface area (~700 m^2/g). Thus in the first heating zone when peroxide was beginning to react with the polymers, nanoclay particles of size 13 μm should be broken into individual sheets (dispersion). These sheets then have to mix effectively (distribution) with the other ingredients in the formulation. Thus a high degree of distributive as well as dispersion mixing was

required in the first heating zone. Figure 4.8 illustrates the dispersion of clay particles into individual clay sheets. Figure 4.9 shows the X-ray diffraction spectra of extrudates. As seen in the spectra, nanoclay was more dispersed in the micro-extruder samples because of absence of the peak at 30-35 A otherwise seen in TX-52 extrudates. However there were no differences among the TX-52 samples eventhough samples from experiment #5 (M configuration, Figure 4.9-b) showed tensile properties equivalent to micro-extruder samples. Thus both distributive and dispersion mixing was enhanced by the presence of kneading discs (M configuration) in the initial stages of heating. Overall M configuration provided more dispersion and/or distribution mixing than F configuration, even as the final nanoclay dispersion in extrudates from both the configurations was the same.

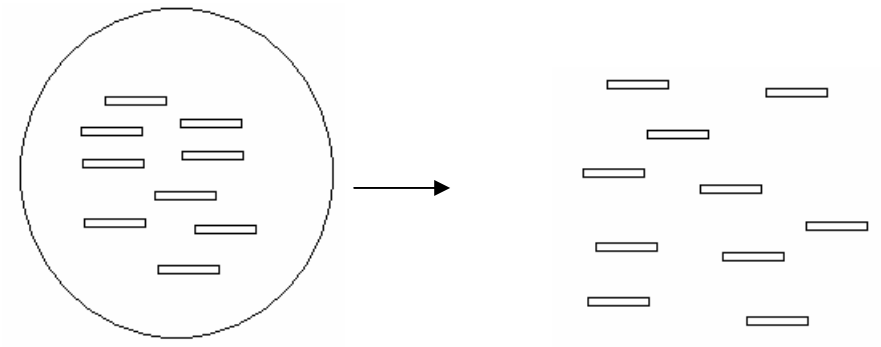

Spherical nanoclay particle of size 13 μm containing > 2000 platelets

Dispersion of clay particle into individual platelets

Figure 4.8: Dispersion of clay particles of size 13 μm into individual clay sheets

Table 4.7 shows the comparison of optimum extrusion parameters in both the micro-extruder and TX-52. Operation of both the extruders within these parameters resulted

in equivalent mechanical properties. The optimum parameters between the two extruders were significantly different.

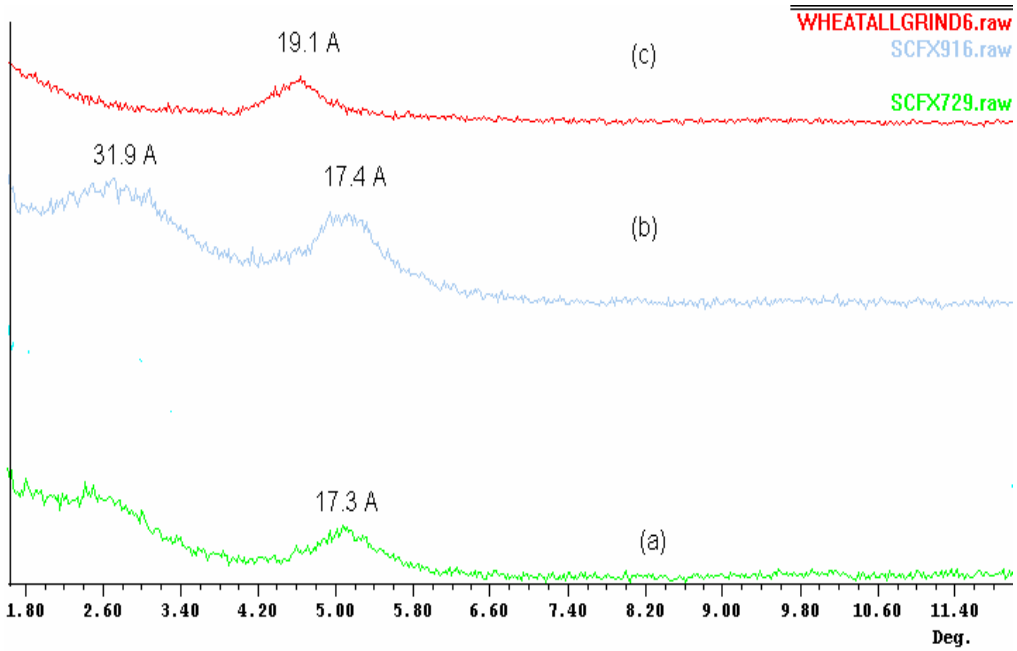

Figure 4.9: X-ray diffraction spectra of extrudates from different screw configurations obtained at low feed rates, low screw speed, and low L/D ratios in TX-52 a) F configuration, b) M configuration and spectra of samples from c) micro-extruder. F-forward screw elements and M-forward and kneading discs

4.4.5 Injection of SC-CO_2

Experiments were also carried out to determine the feasibility of producing low-density foams from starch-PCL reactive blends by a 2-step extrusion process. The first step was the reactive extrusion process carried out with the following parameters: L/D=15, screw speed= 40 rpm (set point), barrel temperatures= 124-126^{0}C (measured) and low feed rates (3-6 kg/hr). A 12 mm cylindrical die was used and a knife cutter was used at 541 rpm to produce thin pellets. As before, the formulation of STPCLPER-6 was used but with H_2O_2 used as a 50% solution in water compared to

>90% solutions used previously. The screw configuration used is illustrated in Figure 4.10-a. A 12-unit kneading disc system staggered at 30^0 forward angle was located near the feed section as shown in Figure 4.10-a.

Table 4.7: A comparison of extrusion parameters in both the micro-extruder and TX-52

Extrusion Parameters	**Micro-Extruder**	**TX-52**
Barrel Temperature, ^{0}C	120	120-125
Product Temperature, ^{0}C	120	129
Set-point Screw Speed, rpm	120	40
Actual Screw Speed, rpm	115	45
Die Shear Rate, s^{-1} *	33.3[a]	5-53[b]
SME, kJ/kg	232.0	291.8
Extrudate Density, kg/m^3	1411	1337.4

a- Die shear rates were calculated by using melt densities of 1204.6 kg/m^3, power law index of 0.34 and micro-extruder output of 0.21 kg/hr

b- Die shear rates were calculated by using melt densities of 1204.6 kg/m^3, power law index of 0.34 and TX-52 output of 3.5 kg/hr (slit die) and 3.0 kg/hr (cylindrical die)

* Die shear rate in cylindrical dies of radius R = $\frac{(3n+1)\,Q}{n\,\pi R^3}$ (reference 20)

Die shear rate in slit dies of width W and height H = $\frac{2(2n+1)Q}{nWH^2}$ (reference 20)

In the second extrusion step, pellets from the first step were fed manually to the feed throat of the extruder. The following extrusion parameters were used: L/D=27, screw speed= 40 rpm (set point), barrel temperatures= $70/120/120/90^0$ C (set-point) and $79/120/116/102^0$ C (measured) in the 4 heads (feed to die), and high feed rates (20.4

kg/hr). The barrel temperatures were measured at L/D = 6, 12, 18 and 24. The product temperature was measured at 137^0C. Feed rate of 20.4 kg/hr was achieved by manually feeding the pellets (obtained from 1st extrusion step) in the extruder. The screw configuration in this extrusion foaming process is illustrated in Figure 4.10-b. A 38.4 x 3.9 mm^2 slit die with die land length of 10 mm was used. SC-CO_2 at 17 MPa was injected into barrel at L/D=24 according to set-up discussed by Rizvi *et al* (21). Flow pressures at L/D=22 and L/D= 26 were measured at 8.1 MPa and 10.2 MPa respectively. These high pressures were generated by use of flow restrictor in the die assembly (between spacer and die holder in Figure 4.4) to adjust flow pressure before the die. The concentration of SC-CO_2 in the melt was 1.1% and 0.2% at the above pressure and temperature conditions.

Tensile and PCL crystal properties of reactively extruded pellets (1st extrusion step) and foam and unfoamed sheets (2nd extrusion step) are illustrated in Table 4.8. Tensile measurements indicated there was no polymer degradation during the second extrusion foaming step. Tensile properties of these samples were similar to those obtained from the first reactive extrusion step (no SC-CO_2 injection). Except for slight reduction in PCL crystallinity of control unfoamed sheets(2nd extrusion step), the melting points were unchanged. This indicated that PCL morphology did not change dramatically during the second extrusion foaming step.

Figure 4.11 shows the digital (a and b) and SEM (c-e) pictures of foamed and unfoamed extrudates from the 2nd extrusion step. Figure 4.11-b showed foams at 1.1% CO_2 exhibiting surfaces similar to those seen in melt-fractured extrudates (22). The

foam density was measured by the method of Tatarka *et al* (23) and was found to be 572 kg/m^3 and 527 kg/m^3 for 0.2% and 1.1% CO_2 levels respectively.

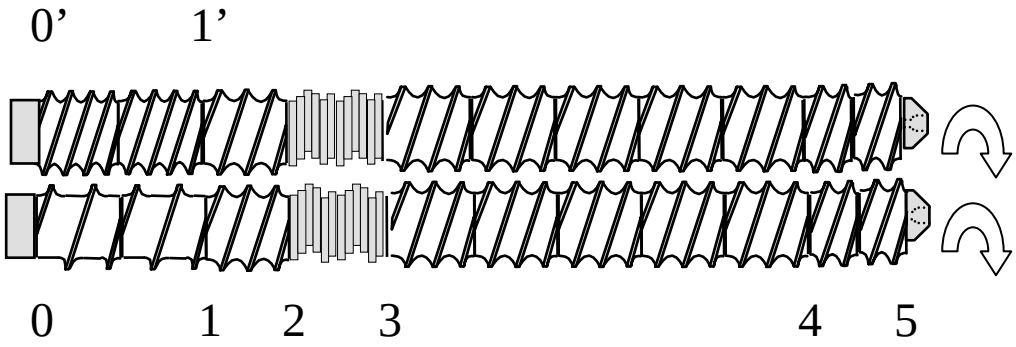

0-1: feed screw of L=156 mm, 0’-1’: feed screw of P= 19 mm and L=156, 1-2: screws of P=26mm and L=78 mm, 2-3: kneading discs of L=72mm, 3-4: screws of P=26mm and L= 390mm, 4-5: screws of P=19mm and L=84mm

(a)

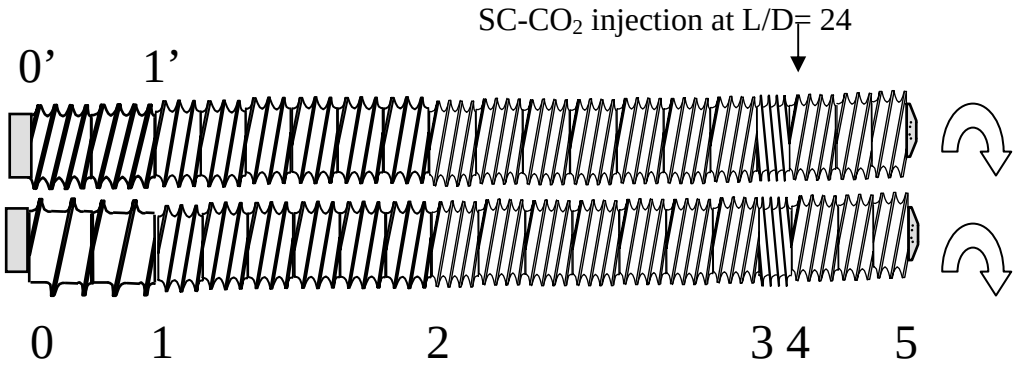

0-1: feed screw of L=156 mm, 0’-1’: feed screw of P= 19 mm and L=156, 1-2: screws of P=26mm and L=468 mm, 2-3: screws of P=19mm and L=546mm, 3-4: reverse screws of P=14mm and L= 71mm, 4-5: screws of P=19mm and L=162mm

(b)

Figure 4.10: Screw configurations for a 2-step extrusion foaming process: a) configuration in the first reactive extrusion step at L/D =15, b) configuration in the second extrusion foaming step at L/D=27 with SC-CO_2 injection at L/D=24. Figures are shown as non-intermeshing eventhough the actual screws are intermeshing. Numbers below the screws indicate the end of screws of a particular type and the beginning of another.

Table 4.8: Tensile and PCL crystal properties (from DSC) of molded samples of reactively extruded pellets from the first extrusion step and foamed and unfoamed sheets from the 2nd extrusion step in TX-52. Foamed sheets contained 1.1% CO_2 at 102^0C and 1500 psi.

Extrusion Step #	**Ultimate Elongation, %**	**Maximum Strength, MPa**	**% PCL Crystallinity**	**PCL Melting Point, ^{0}C**
1 (pellets)	1186[a]	15.0[a]	32.8[a]	55.0[a]
2 (unfoamed sheets)	1323[a]	16.5[b]	30.7[b]	56.0[a]
2 (foamed sheets)	1285[a]	16.6[b]	33.6[a]	55.5[a]

Different alphabets indicate significant mean difference at confidence level 0.95

SEM pictures showed a non-homogeneous distribution of cellular structures (Figures 4.11- d and e). From these pictures and visual observation, foam appearance could be related to solubility of SC-CO_2 in starch-PCL reactive blend. Low SC-CO_2 solubilities led to dissolution of CO_2 during early stages of die flow. This foam would be then subjected to shear along most of the die length. Also there was little difference in foam densities at 0.2% and 1.1% CO_2 levels. The width of foam extrudates with 0.2% CO_2 was approximately 38 mm while that of 1.1% CO_2 foams were 10 mm lesser. This indicated that shearing of expanded polymer melts containing high levels of CO_2 in the die region led to both escape of CO_2 from the surface and edges (small voids seen on extrudate surface/edges in foams with 1.1% CO_2). The foam densities can also be

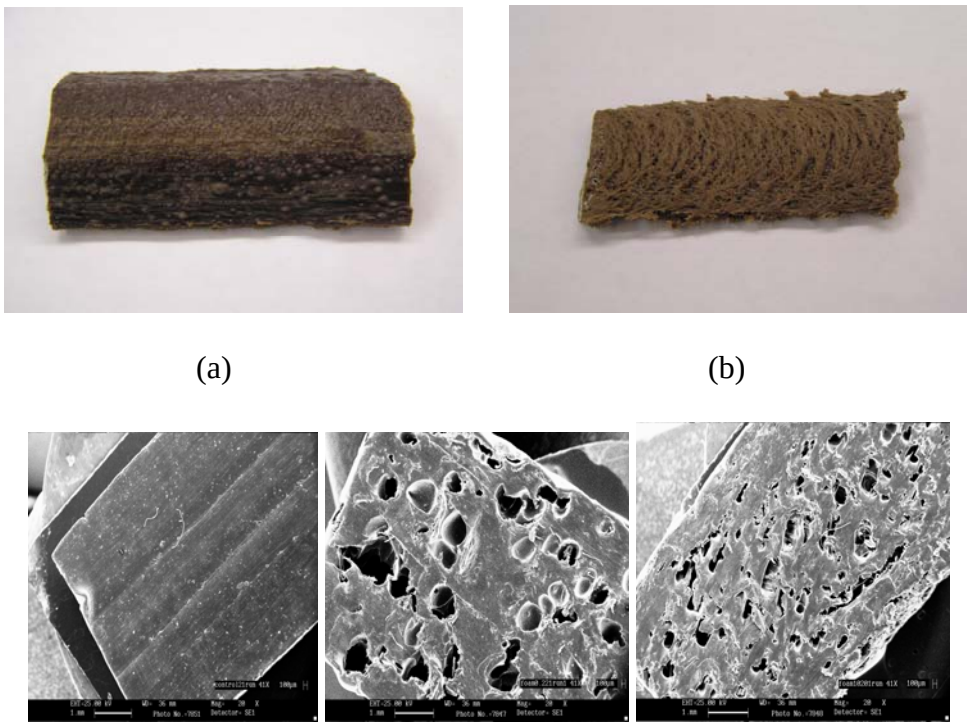

(a) (b)

(c) (d) (e)

Figure 4.11: Digital pictures of TX-52 extrudates of STPCLPER-6 upon injection of SC-CO_2 at a) 0.2% SC-CO_2 and b) 1.1% SC-CO_2. SEM pictures of c) unfoamed extrudates, foams with d) 0.2% CO_2 and e) 1.1% CO_2. The operating pressure and temperature were 10.2 MPa (1500 psi) and 102^0C respectively.

approximately predicted by calculating the volume expansion of CO_2 for a given concentration in the polymer. Table 4.9 shows the calculated melt and foam densities at 137^0C (product temperature) for two CO_2 levels. Density of melts containing polymers and SC-CO_2 was calculated at 10.2 MPa using weighted average of individual densities. Foam density was calculated at atmospheric pressure from polymer melt density and CO_2 expansion. Experimental foam densities are also listed for the two CO_2 levels. At 0.2% and 1.1% CO_2 levels used in STPCLPER-6 formulation, the foams were expected to have densities of 423 kg/m^3 and 108 kg/m^3 respectively. The calculated density value at 0.2% CO_2 level was closer to the

experimental value, but was still significantly lower. The lower calculated density at 1.1% CO_2 level indicated that residence time after SC-CO_2 injection might not be sufficient to allow complete solubilization of the supercritical fluid into the polymer melt.

Table 4.9: Calculated melt and foam densities of STPCLPER-6 containing two levels of CO_2 and their comparison with experimental foam density measured at ambient conditions. Density of melts containing polymers (1204 kg/m^3) and SC-CO_2 was calculated at 137^{0}C and 10.2 MPa while the foam density was calculated at 137^{0}C and atmospheric pressure. Density of SC-CO_2 at 137^{0}C and 10.2 MPa was 150 kg/m^3 (24).

CO_2 Concentration (wt%)	**Calculated Melt Density (kg/m^3)**	**Calculated Foam Density (kg/m^3)**	**Experimental Foam Density (kg/m^3)**
0.2	1202	423	572
1.1	1191	108	527

4.5 Recommendations

Scale-up studies discussed here were successful only at lower feed rates while higher feed rates resulted in poor tensile properties. Commercial operations can only be economically viable when the extruders are operated at higher throughputs. A venting system needs to be used to remove moisture at higher operating feed rates. We have not carried out any venting studies because of limited supply of expensive PCL. In the case of a venting system being used, the location of such a system and screw configuration were expected to be two new independent variables that would affect material properties.

A high-pressure study on SC-CO_2 solubility in polybutylene succinate (PBS, see structure in chapter 1, Figure 1.1) estimated 7.5% CO_2 solubility in 100% PBS at ~8.8 MPa and 120^0C (26). This translated into approximately 2.8% SC-CO_2 solubility in STPCLPER-6 formulation assuming same solubility levels between PCL and PBS. Future studies need to determine actual SC-CO_2 solubility in the formulation and the effect of allowing additional time to solubilize SC-CO_2 in the melt (e.g. use of static mixers). Also additional reverse screws and a conical head at the end can increase flow pressures thus allowing incorporation of higher levels of SC-CO_2. An increase in pressure can also increase the density of SC-CO_2 from 150 kg/m^3 (at 10.2 MPa and 137^0C) leading to better mixing between the polymer and the supercritical fluid.

4.6 Conclusion

Reactive extrusion process based on starch-PCL blends was successfully scaled up from a batch-type conical micro-extruder to a continuous parallel twin-screw extruder (TX-52) in FPDL. The optimum process parameters in the two extruders were different. Best tensile properties in the TX-52 were obtained at a low screw speed of 40 rpm compared to optimum value of 120rpm in the micro-extruder. Special mixing elements (forward kneading discs) in the initial section of TX-52 were found to produce extrudates with tensile properties similar to those from micro-extrusion. Injection of SC-CO_2 into the polymer melts during the TX-52 extrusion process was attempted. The resulting foams showed a non-homogenous cellular structure and appeared to show brittle behavior compared to unfoamed material.

4.7 References

1. Bigio, D., Cassidy, K., Dellapa, M., Baim, W., International Polymer Processing, vol. VII, 111 (1992).

2. Kim, B.J., White, J.L., International Polymer Processing, vol. XVII, 33 (2002).

3. Poulesquen, A., Vergnes, B., Cassagnau, Ph., Gimenez, J., Michel, A., International Polymer Processing, vol. XVI, 31 (2001).

4. Mani, R., Bhattacharya, M., European Polymer Journal, vol. 3737:515 (2001).

5. Narayan, R., Krishnan, M., Snook, J.B., Gupta, A., DuBois, P., US Patent# 5,906,783 (1999).

6. Riaz, M., Extruders in Food Applications, Technomic Publishing Co., Lancaster, PA (1997).

7. Tadmor, Z., Gogos, C.G., Principles of Polymer Processing, John Wiley & Sons, NY-USA (1979).

8. Zuilichem, D.J.V., Kuiper, E., Stolp, W., Jager, T., Powder Technology, vol. 106, 147 (1999).

9. Kim, B., White, J.L., Polymer Engineering and Science, vol. 37, 576 (1997).

10. Tzonganakis, C., Vlachopoulos, J., Hamielec, A.E., International Polymer Process, vol. 3, 141 (1988).

11. Strutt, D., Tzoganakis, C., Duever, T.A.: SPE ANETC Tech. Papers, 227 (1998).

12. Berzin, F., Vergnes, B., Dufosse, P., Delamare, L., Polymer Engineering and Science, vol. 40, 344 (2000).

13. Mange, C., Boissonnat, P., in Extrusion Technology for the Food Industry, ed. Connor, C.O., pg. 117, Elsevier Science Publishing CO., NY-USA (1987).

14. Haley, T.A., Mulvaney, S.J., Food Control, vol. 11, 103 (2000).

15. Rauwendaal, C., ANTEC-2000. (see copy in http://www.rauwendaal.com/)

16. Martin, O., Averous, L., Della Valle, G., Carbohydrate Polymers, vol. 53, 169 (2003).

17. Ishikawa, T., and Amano, T., Kihara, S.I., Funatsu, K., Polymer Engineering and Science, vol. 42, 925 (2002).

18. Shearer, G., Tzoganakis, C., Polymer Engineering and Science, vol. 41, 2206 (2001).

19. Shearer, G., Tzoganakis, C., Polymer Engineering and Science, vol. 40, 1095 (2000).

20. Crawford, R.J., Plastics Engineering, pg. 55, Elsevier Reed Plc, Woburn, MA (1998).

21. Rizvi, S.S.H., Extrusion Processing with Supercritical Fluids, US Patent 5120559 (1992).

22. Benbow, J., Bridgwater, J., Flow defects and phase migration, chap. 7, in Paste Flow and Extrusion, Clarendon Press, Oxford (1993).

23. Tatarka, P.D., Cunningham, R.L., Journal of Applied Polymer Science, vol. 67, 1157 (1998).

24. Reid, R.C., Prausnitz, J.M., Poling, B.E., The Properties of Gases and Liquids, 4th ed., McGraw-Hill, NY (1987).

25. Sato, Y., Takikawa, T., Sorakubo, A., Takishima, S., Masuoka, H., Imaizumu, M. Industrial Engineering Chemistry Research, vol. 39, 4813 (2000).